POLITECNICO DI TORINO
Repository ISTITUZIONALE

Bio-based isobornyl polymer matrices for transparent wood: optical, thermal, and mechanical trade-offs

Original
Bio-based isobornyl polymer matrices for transparent wood: optical, thermal, and mechanical trade-offs / Cabras, A., Nuvoli, D., Malucelli, G., Pugliese, D., Terzi, M., Konigsberger, M., Schindler, J., Mariani, A.. - In: COMPOSITES. PART A, APPLIED SCIENCE AND MANUFACTURING. - ISSN 1878-5840. - ELETTRONICO. - 212:(2027), pp. 1-12. [10.1016/j.compositesa.2026.110316]

Availability:
This version is available at: 11583/3016137 since: 2026-09-30T08:53:37Z

Publisher:
Elsevier

Published
DOI:10.1016/j.compositesa.2026.110316

Terms of use:

This article is made available under terms and conditions as specified in the corresponding bibliographic description in the repository

Publisher copyright

(Article begins on next page)

18 November 2026

Composites: Part A 212 (2027) 110316

Contents lists available at ScienceDirect

Composites Part A

journal homepage: www.elsevier.com/locate/compositesa

Bio-based isobornyl polymer matrices for transparent wood: optical, thermal, and mechanical trade-offs

Alessia Cabras [a], Daniele Nuvoli [a,*], Giulio Malucelli [b], Diego Pugliese [c], Marco Terzi [d], Markus Königsberger [e], Johanna Schindler [e], Alberto Mariani [a]

[a] Department of Chemical, Physical, Mathematical, and Natural Sciences, and local INSTM unit, University of Sassari, Via Vienna 2, Sassari 07100, Italy
[b] Department of Applied Science and Technology, Politecnico di Torino, Viale T. Michel 5, Alessandria 15121, Italy
[c] Division of Applied Metrology and Engineering, National Institute of Metrological Research (INRiM), Strada delle Cacce 91, Torino 10135, Italy
[d] Division of Quantum Metrology and Nanotechnologies, National Institute of Metrological Research (INRiM), Strada delle Cacce 91, Torino 10135, Italy
[e] Institute of Mechanics of Materials and Structures, Vienna University of Technology, Karlsplatz 13/202, Vienna 1040, Austria

HIGHLIGHTS

- Isobornyl-based matrices matched the refractive index of delignified wood.
- Copolymer composition controlled transparency and haze in TW.
- The three copolymer formulations exhibited comparable transmittance near 80 %
- Thermal conductivity remained low (0.15–0.18 $W \cdot m^{-1} \cdot K^{-1}$) across formulations.
- IBOA-rich copolymers provided the most balanced multifunctional response.

ARTICLE INFO

Keywords:
Transparent wood
Bio-based polymers
Optical properties
Biocomposite material

ABSTRACT

Transparent wood was prepared by infiltrating delignified balsa templates with bio-based isobornyl acrylate (IBOA) and isobornyl methacrylate (IBOMA) matrices, including the corresponding homopolymers and three copolymer compositions. The formulations were compared in terms of refractive index, optical transmittance, haze, thermal conductivity, bending response, and ultrasonic stiffness components. All samples showed high visible transmittance at 550 nm, ranging from 69 to 80 %, while haze remained substantial due to scattering within the anisotropic wood structure. Copolymerization improved the optical balance relative to the homopolymers: the three copolymer compositions showed comparable transmittance, whereas the 0.25/0.75 (IBOA/IBOMA) and 0.75/0.25 compositions exhibited lower haze than the 0.50/0.50 composition. Thermal conductivity varied only slightly (between 0.15 and 0.18 $W \cdot m^{-1} \cdot K^{-1}$), indicating that heat transport was mainly controlled by the wood-polymer architecture. Bending tests showed that IBOA-rich systems provided the most favorable mechanical response. An exploratory optical-mechanical desirability comparison indicated that the 0.75/0.25 copolymer offered the most balanced optical and mechanical profile within the investigated set.

Introduction

Transparent wood (TW) is an innovative composite material in which the lignocellulosic structure of wood is impregnated with a transparent polymer. Its distinguishing feature is the combination of high optical transmittance with the favorable mechanical properties arising from the preservation of wood's cellular architecture. Conventional transparent materials such as glass and polymers generally do not provide the same combination of strength, toughness, low density, and impact resistance, while structural materials with comparable mechanical performance are typically opaque. Its renewable origin further strengthens its relevance for applications requiring both optical and structural functionality. Potential uses span from construction [1], architecture [2], design of solar cells [3], electronic devices [3], thermal insulation [4], and energy storage systems [3,4].

The fabrication of TW involves an initial treatment to either remove

* Corresponding author.
E-mail address: dnuvoli@uniss.it (D. Nuvoli).

https://doi.org/10.1016/j.compositesa.2026.110316
Received 22 July 2026; Received in revised form 24 September 2026; Accepted 25 September 2026
Available online 26 September 2026
1359-835X/© 2026 The Author(s). Published by Elsevier Ltd. This is an open access article under the CC BY license (http://creativecommons.org/licenses/by/4.0/).

(delignification) or chemically modify (bleaching) lignin, the component containing chromophoric groups responsible for wood's natural coloration. Subsequently, the treated templates are impregnated with a suitable monomer that, upon polymerization/curing, gives rise to a matrix with a refractive index (RI) matching that of the delignified wood scaffold [1]. This RI matching significantly reduces light scattering at the microstructural interfaces, thereby achieving high optical transparency. Conventional production methods predominantly employ epoxy resins or petroleum-based synthetic polymers, such as poly (methyl methacrylate) (PMMA), due to their superior optical and mechanical performance [5,6]. A widely used system is based on diglycidyl ether of bisphenol A (DGEBA), often modified with ethylene glycol diglycidyl ether to enhance flexibility [7]. Despite its efficacy, DGEBA is derived from bisphenol A, a compound associated with environmental toxicity and adverse effects on human health [8,9]. To mitigate these issues, recent research has explored water-soluble alternatives like polyvinyl alcohol [4] and polyvinylpyrrolidone [10,11], which, while offering biocompatibility and partial biodegradability, are synthesized from fossil-derived materials.

The quest for sustainability has driven the development of entirely or predominantly bio-based matrices. For instance, poly(limonene acrylate), derived from agro-industrial waste, provides transparent wood with optical transmittance and mechanical strength comparable to PMMA [12]. Other studies have utilized poly(lactic acid) in combination with cellulose nanocrystals to develop sustainable nanocomposites [13]. Furthermore, fully bio-based approaches involving delignified wood impregnated with cellulose nanofibers and chitosan have shown high optical transmittance and enhanced thermal stability [14].

In this study, we propose the use of bio-based polymers from the isobornyl family, specifically referring to poly(isobornyl acrylate) (polyIBOA) and poly(isobornyl methacrylate) (polyIBOMA) to fabricate TW, as bio-based alternatives to conventional fossil-derived matrices. These polymers are characterized by high renewable carbon content, reaching approximately 75% for polyIBOA [15] and up to 80% for polyIBOMA [16,17]. Chemically, isobornyl acrylate (IBOA) and isobornyl methacrylate (IBOMA) monomers are obtained via esterification of isoborneol, a cyclic terpenic alcohol derived from pine resin or camphor [18,19]. Sustainable synthesis routes have already been established for these monomers, utilizing solid acid catalysts like Amberlyst-15 or zirconium-based superacids to enable solvent-free reactions at moderate temperatures [19,20]. Although these polymers are widely employed in coatings and adhesives [16], their application in TW fabrication remains unexplored in the literature. PolyIBOA and polyIBOMA were selected not only for their renewable origin but also for their favorable physical properties. Furthermore, polyIBOA provides toughness and flexibility [21,22], while polyIBOMA offers excellent thermal stability and resistance to high temperatures [23,24]. Consequently, this work investigates the optical, mechanical, morphological and thermal characteristics of TW infiltrated with polyIBOA and polyIBOMA homopolymers, as well as various copolymers (polyIBOA molar fractions of 0.25, 0.50, and 0.75), to evaluate their potential as bio-based matrices for TW.

Materials and methods

Materials

For the fabrication of TW, balsa wood veneers with a thickness of 1.0 mm were used, which were obtained from matèria PRIMA (materiaprimashop.com). Sodium chlorite (purity = 80%, $d = 2.43$ g/cm^3, MW = 90.44 g/mol), glacial acetic acid (purity ≥ 99.7%, $d = 1.049$ g/mL, MW = 60.05 g/mol), isobornyl acrylate (IBOA, purity ≥ 85%, $d = 0.986$ g/mL, MW = 208.30 g/mol, containing 200 ppm of monomethyl ether of hydroquinone), isobornyl methacrylate (IBOMA, purity = 85%, d = 0.983 g/mL, MW = 222.32 g/mol) and diphenyl(2,4,6-trimethylbenzoyl) phosphine oxide (TPO, photoinitiator; λ_{max} = 380 nm, purity ≥ 96.5%, MW = 348.37 g/mol) were purchased from Sigma-Aldrich. Sodium acetate (purity > 99%, MW = 82.04 g/mol) was supplied by Fluka Chemicals. Absolute ethanol (purity = 99.9% $d = 0.79$ g/mL, MW = 46.07 g/mol) and acetone (purity = 99%, $d = 0.79$ kg/L, MW = 58.08 g/mol) were supplied by VWR Chemicals. All reagents were used as received, except for the IBOA monomer, from which the inhibitor was removed using an alumina separation column.

Samples preparation

Delignification

Balsa wood samples with a thickness of 1.0 mm were cut into two sizes, namely: 4×4 cm^2 and 1.5×8 cm^2. The samples were immersed in a buffer solution at pH 4.6, prepared by dissolving 0.4 g of sodium acetate and adding 0.3 mL of acetic acid per 100 mL of solution. A volume of 12 mL of buffer solution was used for each gram of wood. Subsequently, sodium chlorite was added at a concentration of 1% (w/v). The delignification process was carried out at 80 °C for 18 h. After the treatment, the samples underwent the following washing cycle using an ultrasonic bath: three consecutive washes with distilled water, followed by three washes with ethanol, and finally three washes with acetone. Each washing step lasted 30 min.

Transparent wood preparation

The delignified and previously washed wood was immersed in a solution containing IBOA and the photoinitiator TPO (0.3 wt.%) and left to infiltrate at 30 °C for 24 h. The same procedure was applied using IBOMA with TPO (0.3 wt.%). For the preparation of copolymers, three different solutions of mixed IBOA and IBOMA were used, varying the molar fraction of IBOA (0.25, 0.50, and 0.75). The infiltrated samples were exposed to ultraviolet (UV) radiation (λ = 395 nm) for 10 to 15 min. Photopolymerization was carried out using the OmniCure® LX500 UV LED Spot Curing System Controller (Excelitas Technologies), equipped with Intelli-Lamp® technology. All the sample were stored in polyethylene bags under lab conditions (T=22 ± 1 °C, RH = 35-45%).

Characterization

Rheological tests

Rheological measurements were performed using an ARES (TA Instrument, New Castle, DE, USA) strain-controlled rheometer equipped with a bob and cup (bob diameter: 40 mm, cup diameter: 42 mm, cup height: 1.5 mm). Strain sweep tests were carried out at 30 and 50 °C; the strain amplitude was set at 1%, and the frequency range was between 100 and 1 rad/s.

Differential scanning calorimetry analyses

Differential scanning calorimetry (DSC) analyses were carried out using a QA1000 TA Instrument apparatus (Waters Lc, Milford, MA, USA). All the experiments were performed under dry N_2 gas (20 mL/min), using samples of around 15 mg of the homopolymers and copolymers in sealed aluminum pans. All the materials were subjected to the following cycle: (i) first heating up from 0 to 180 °C at 10 °C/min; (ii) cooling down from 180 to 0 °C at 10 °C/min; (iii) second heating up from 0 to 180 °C at 10 °C/min. The glass transition temperature (T_g) values were calculated on the second heating up curve.

FTIR spectroscopy

Fourier-transform infrared (FTIR) spectra were acquired using a Jasco FT-IT-4600 spectrometer (Jasco Corp., Tokyo, Japan) in the spectral range of 4000–500 cm^{-1}. Each spectrum was obtained at a resolution of 4 cm^{-1} by averaging 32 scans. A background spectrum was collected under the same conditions before each measurement.

Refractive index

The refractive indices of the delignified wood, polymer and

copolymer thin films were determined using an Abbe refractometer (AR4, A. KRÜSS Optronic GmbH). To ensure proper optical coupling between the thin-film samples and the measuring prism, cinnamon oil (commercially labeled as Zimtöl with approximate refractive index of 1.59) was used as the contact medium. All measurements were performed at a stabilized temperature of 20.6 °C.

UV-visible analysis

Optical transmittance and haze were measured using an ultraviolet–visible–near-infrared (UV–Vis–NIR) spectrophotometer (Agilent Cary 5000, Agilent Technology, Santa Clara, CA, USA), equipped with an integrating sphere, allowing simultaneous collection of directly transmitted and forward-scattered light. Transmittance spectra were acquired in the 300-900 nm range, while haze measurements were performed in the visible region (380-780 nm) according to ASTM D1003 [25].

Prior to measurements, a 100% transmission reference (WHITE, W) and a 0% baseline (DARK, D) were recorded. Samples were mounted at the entrance port of the integrating sphere with perpendicular alignment to the incident beam and complete coverage of the aperture. Instrumental parameters, including spectral bandwidth, scan rate, and data interval, were kept constant for all measurements to ensure reproducibility.

The total transmitted signal (S), including both ballistic and scattered contributions, was used to calculate the spectral transmittance (T) according to Eq. (1):

$$T = \frac{S - D}{W - D} \tag{1}$$

Haze was evaluated using the same integrating sphere configuration from four independent signals: (i) T_1, reference signal without sample using a white standard; (ii) T_2, total transmitted light through the sample; (iii) T_3, instrumental scattering measured without sample using a light trap; and (iv) T_4, diffuse transmitted light measured with both sample and light trap.

The haze value was calculated as shown in Eq. (2):

$$\text{Haze} = \frac{T_d}{T_t} = \left(\frac{T_4}{T_2} - \frac{T_3}{T_1}\right) \times 100\% \tag{2}$$

where T_d is the diffuse transmittance and T_t is the total transmittance. All measurements were performed along the longitudinal direction of the wood structure, and reported values correspond to the average of three independent replicates.

SEM analysis

The morphological and microstructural features of the prepared TW samples were examined using a ZEISS EVO 50 XVP SEM (Oberkochen, Germany) at 10 kV of source potential; before SEM analysis, the samples were coated with a conductive layer of gold.

Thermal conductivity

The thermal conductivity (k) measurements were performed according to ISO 22007-2:2022 [26], using the transient plane source (TPS) method with a Hot Disk TPS 2500S apparatus (Hot Disk AB, Göteborg, Sweden), equipped with a Kapton sensor of 3.189 mm radius. The TPS method employs a planar, disk-shaped sensor that serves simultaneously as a heat source and a thermometer. When a short electrical pulse is applied, the sensor's temperature rises, and this transient response is recorded. By fitting the temperature *vs.* time curve to the theoretical heat diffusion model, the k of the sample can be derived. The direction of thermal conductivity tests was radial, i.e. the thermal parameter was evaluated through the sample's thickness. All measurements were conducted under controlled laboratory conditions (23 ± 1 °C, 50 ± 5 % RH). Each measurement was repeated three times on each sample to estimate the experimental uncertainty, which was within ± 3 %.

Four-point bending test

Mechanical bending tests were performed to quantify the bending stiffness E_b and bending strength σ_b of the material. The tests were carried out on an ElectroForce Bose 3200 test bench (TA Instruments, New Castle, DE, U.S.) using a custom-made four-point bending setup. It consists of two aluminum rails with adjustable three-dimensional (3D)-printed supports made of carbon fiber-reinforced polyphthalamide (PPA), on which aluminum bearings were placed to support the sample from below and load the sample from above. A 3D-printed centering device was used to align the sample with the aluminum rails and ensure central load application.

To measure the bending stiffness, a total force F of 1 N was applied (within 1 min) using a 450 N load cell. This comparatively low load was selected because it already produced midspan deflections of approximately 0.1 mm, while minimizing the risk of premature damage in the brittle polymer-containing specimens. Deflections δ were recorded using a linear variable differential transformer (LVDT) sensor positioned at midspan below the sample.

The effective bending stiffness $(EI)_{\text{eff}}$ from the four-point bending test was then obtained from Euler–Bernoulli beam theory as (Eq. (3):

$$(EI)_{\text{eff}} = \frac{F}{\delta}\left(\frac{al^2}{16} - \frac{a^3}{12}\right) \tag{3}$$

where l is the span (length between the two outer supports), a is the distance between the load application and the support. To obtain the sought elastic modulus, the sandwich-type nature of the samples is taken into account. Microscopic analysis revealed that polymer-rich surface layers may be present on both the upper and lower sides of the specimens, as shown in Fig. 1. The thickness of these polymer layers (h_{top}, h_{bottom}) ranged between 0.05 and 0.25 mm. To eliminate the influence of these layers and quantify the actual bending stiffness of the TW core, laminate theory was adopted [27], assuming linear elastic material behavior, perfect bonding between the layers, and small deflections, so that Euler–Bernoulli beam theory remains valid. The effective bending stiffness can then be decomposed into the contribution of the polymer-rich surface layers and the TW core as (Eq. (4)

$$(EI)_{\text{eff}} = E_{\text{poly}} I_{\text{poly}} + E_{\text{core}} I_{\text{core}} \tag{4}$$

where E_{poly} is the modulus of the polymer layers, E_{core} is the unknown modulus of the TW core, and I_{poly} and I_{core} are the corresponding second moments of inertia with respect to the neutral axis, quantified by considering a potential asymmetric layer configuration using microscopy-measured layer thicknesses h_{top} and h_{bottom}, and a constant core thickness h_{core}. The elastic modulus of the polymer surface layers E_{poly} is generally unknown. For IBOA, nanoindentation tests were performed on the same samples within the polymer-filled lumen to obtain in situ stiffness measurements. Assuming an isotropic phase and a typical polymer Poisson's ratio of 0.4, the resulting Young's modulus of IBOA, E_{IBOA}, amounted to 3.79 GPa. Since no direct indentation value was available for IBOMA, its modulus was approximated from the ratio

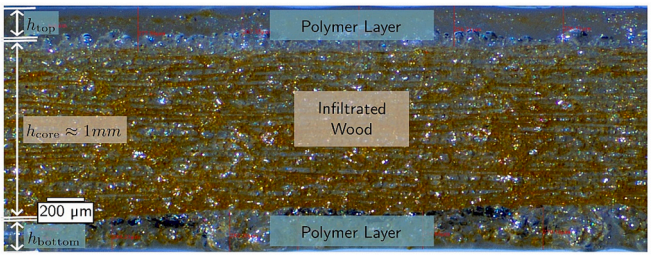


Fig. 1. Cross section of sandwich-type TW samples used for bending tests.

of the bending test results as $E_{IBOMA} = 0.74\ E_{IBOA}$ as a best estimate. This estimate is not fully independent from the bending data and may therefore introduce some circularity in the correction procedure. To account for this uncertainty, the sensitivity of the corrected TW-core modulus is evaluated by varying E_{IBOMA} between $0.5{\cdot}E_{IBOA}$ and $1.0{\cdot}E_{IBOA}$, corresponding to E_{IBOMA} = 1.90 - 3.79 GPa. This range is chosen as a conservative estimate, since the modulus of IBO(M)A-based samples is expected to remain below that of PMMA, which is approximately 2 Gpa [28]. For co-polymer mixtures, E_{poly} was calculated using a linear rule of mixtures based on the respective volume fractions of E_{IBOA} and E_{IBOMA}. The resulting E_{core} ranges represent model-sensitivity intervals and not statistical confidence intervals. The apparent whole-specimen modulus E_{total}, which does not require an assumed constituent modulus, was retained as the primary bending result.

Using the measured geometry parameters b, l, a, h_{top}, h_{bottom}, and h_{core}, the applied force F, the measured deflection δ, and the independently determined modulus of the polymer-rich layers E_{poly}, the bending modulus of the TW core (E_{core}) was quantified. Since the position of the neutral axis depends on the ratio between E_{core} and E_{poly}, the resulting implicit formulation was solved iteratively. For reference, an apparent bending modulus of the whole samples was additionally determined, using $(EI)_{eff} = E_{total}I_{total}$, with $I_{total} = b(h_{bottom} + h_{core} + h_{top})^3/12$.

For the strength tests, the same setup was used albeit with displacement-controlled loading until complete failure at $F = F_{max}$ with a speed of 0.1 mm/s. The bending strength σ_b was calculated as (Eq. (5):

$$\sigma_b = \frac{3F_{max}a}{bh_{eff}^2} \tag{5}$$

Eq. (5) was evaluated using two different thickness definitions h_{eff}. First, the total specimen thickness, $h_{eff} = h_{bottom} + h_{core} + h_{top}$ was used to obtain the apparent bending strength of the complete specimen in its tested configuration. Second, the thickness of the transparent wood core, $h_{eff} = h_{core}$, was used to estimate the nominal bending stress associated with the core region alone. The latter approach neglects the possible load-bearing contribution of the surface layers and therefore provides a higher estimate of the core-related nominal bending strength.

Ultrasound testing

A single-element transducer operating at 5 MHz was employed for ultrasound testing. The ultrasonic waves were generated using an ultrasonic pulser/receiver (PR 5077, Panametrics Inc., Billerica, Massachusetts, U.S.), and the time-of-flight was measured manually, aided by a digital oscilloscope (WaveRunner 62Xi, Lecroy Corporation, Chestnut Ridge, New York, U.S.). The setup consisted of the sample, placed between the sender and the transducer with honey as a coupling medium, and a plastic foil layer as a protection. A baseline measurement was conducted without the sample to determine the time-of-flight through the setup itself [29].

Using longitudinal and transversal transducers allows for quantifying three different stiffness components, all by sending the ultrasonic wave through the thickness direction, i.e. in radial (r) direction with respect to the wood's orthotropic coordinate system. Therefore, the wave velocity of longitudinal P-waves ($v_{l,rr}$) and transversal S-waves ($v_{t,rl}$ for particles moving in l-direction and $v_{t,rt}$ for particles moving in t-direction) are determined first by dividing the travel distance of the wave, the sample thickness $h_{bottom} + h_{core} + h_{top}$, by the corresponding measured time-of-flight t_f (corrected by the baseline time-of-flight), reading as (Eq. (6):

$$v = \frac{h_{bottom} + h_{core} + h_{top}}{t_f} \tag{6}$$

The radial normal stiffness tensor component C_{rrrr} then follows from the density ρ and from the corresponding wave velocity as $C_{rrrr} = \rho v_{l,rr}^2$. By analogy, the shear stiffness components C_{rlrl} and C_{rtrt} follow from the corresponding transversal wave velocities as $C_{rlrl} = \rho v_{t,rl}^2$ and $C_{rtrt} = \rho v_{t,rt}^2$.

Results and discussion

Given that the infiltrating polymer dictates the composite's final properties, its careful selection is pivotal for optimizing TW composites for specific applications. Understanding material performance necessitates multiple approach: rheological analysis of the monomers to characterize flow behavior and processability, complemented by DSC on cured samples to elucidate thermal properties, FTIR analysis to confirm the conversion of monomer to polymer and refractive index analysis to assess its proximity to the literature reference for the delignified wood scaffold.

Rheology measurements

Fig. 2 shows the complex viscosity *vs.* angular frequency for the two monomers, at two different temperatures (i.e., 30 and 50 °C). At low shear rates, both monomers exhibit approximately Newtonian behavior, which is characterized by nearly constant viscosity, independent of the applied shear rate. This suggests that the molecular arrangement is mostly unaffected by the flow field and that the resistance to deformation is predominantly governed by the intrinsic viscosity of the monomers. As the shear rate increases, both the monomers progressively deviate from Newtonian behavior and exhibit a shear-thinning behavior, with viscosity values decreasing as the shear rate increases. The shear-thinning behavior can be ascribed to the progressive alignment of molecular structures along the flow direction, which reduces intermolecular friction and facilitates the flow. The onset and extent of shear thinning become more evident at higher shear rates, where the applied deformation is sufficient to modify the microstructural organization of the liquid monomers.

In addition to the shear-rate dependence, a strong temperature effect is observed. For both monomers, the complex viscosity decreases continuously with increasing temperature: this is ascribed to improved molecular mobility and decreased intermolecular interactions. A comparison of the rheological behavior of the two monomers reveals that IBOMA exhibits higher viscosity values than IBOA across the entire temperature range investigated. The higher viscosity of IBOMA is ascribed to the presence of the additional -CH_3 group in the methacrylate structure, which increases steric hindrance, hence restricting molecular mobility.

In conclusion, the monomers exhibited low complex viscosity values, resulting in low resistance to flow. This rheological behavior facilitates their penetration into the porous structure of the delignified wood, and thereby favor effective impregnation of the wood scaffold.

DSC

The first heating ramp performed on IBOA and IBOMA polymers and their respective copolymers did not show any exothermic peak due to residual polymerization of the monomers, confirming that the conversion of the monomers was close to 100% for all the investigated compositions. The T_g values of the investigated polymeric formulations used in this work are collected in Table 1. They show a clear dependence on the polyIBOA/polyIBOMA ratio, confirming that the comonomer composition affects the thermal mobility of the polymer phase within the TW. For TW with IBOMA, the glass transition is not evident; conversely, the TW infiltrated with the copolymers show well-defined T_g values. In particular, the highest T_g (i.e., 133 °C) is observed for TW - poly(IBOA-co-IBOMA) 0.75/0.25. Within the copolymer series, T_g increases from 94 °C for the 0.25/0.75 composition to 116 °C for the 0.50/0.50 composition and 133 °C for the 0.75/0.25 composition. The observed composition dependence cannot be interpreted solely from the

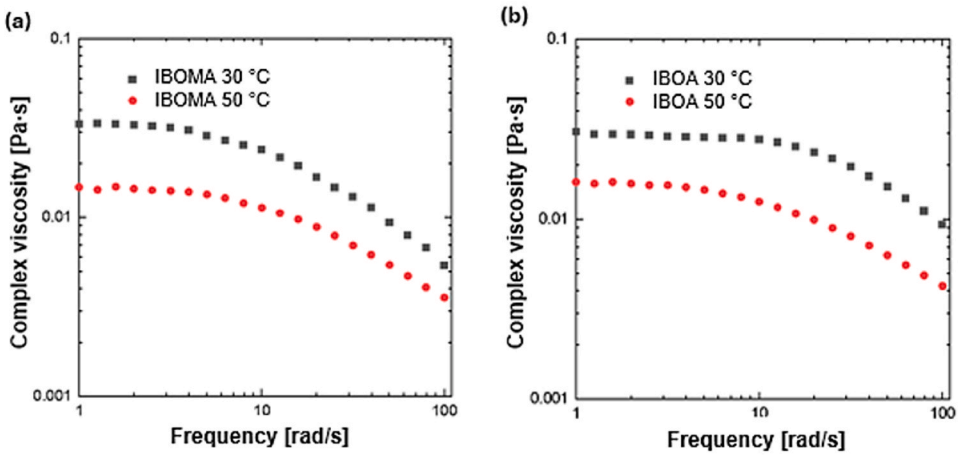


Fig. 2. Complex viscosity *vs.* angular frequency for IBOMA (a) and IBOA (b), at 30 and 50 °C.

Table 1
T_g and refractive index values of the TW samples.

Polymer	T_g [°C]	Refractive index
PolyIBOMA	Not evident	1.493
Poly(IBOA-co-IBOMA) 0.25/0.75	94	1.492
Poly(IBOA-co-IBOMA) 0.50/0.50	116	1.492
Poly(IBOA-co-IBOMA) 0.75/0.25	133	1.498
PolyIBOA	104	1.493

structural difference between IBOA and IBOMA and may also reflect copolymer microstructure and polymerization-related effects.

Interestingly, the TW - polyIBOA sample shows a T_g of 104 °C, which is slightly higher than the poly(IBOA-co-IBOMA) 0.25/0.75 composition. Together with the copolymer values, this confirms that T_g does not follow a simple linear mixing rule and may be influenced by factors such as polymerization kinetics, copolymer microstructure, molar mass, and wood-polymer interactions [30].

Although DSC analyses were employed specifically for evaluating the T_g of the TW systems, they also indicated that the prepared TWs are thermally stable up to 200°C, that represents a more than acceptable value for structural applications.

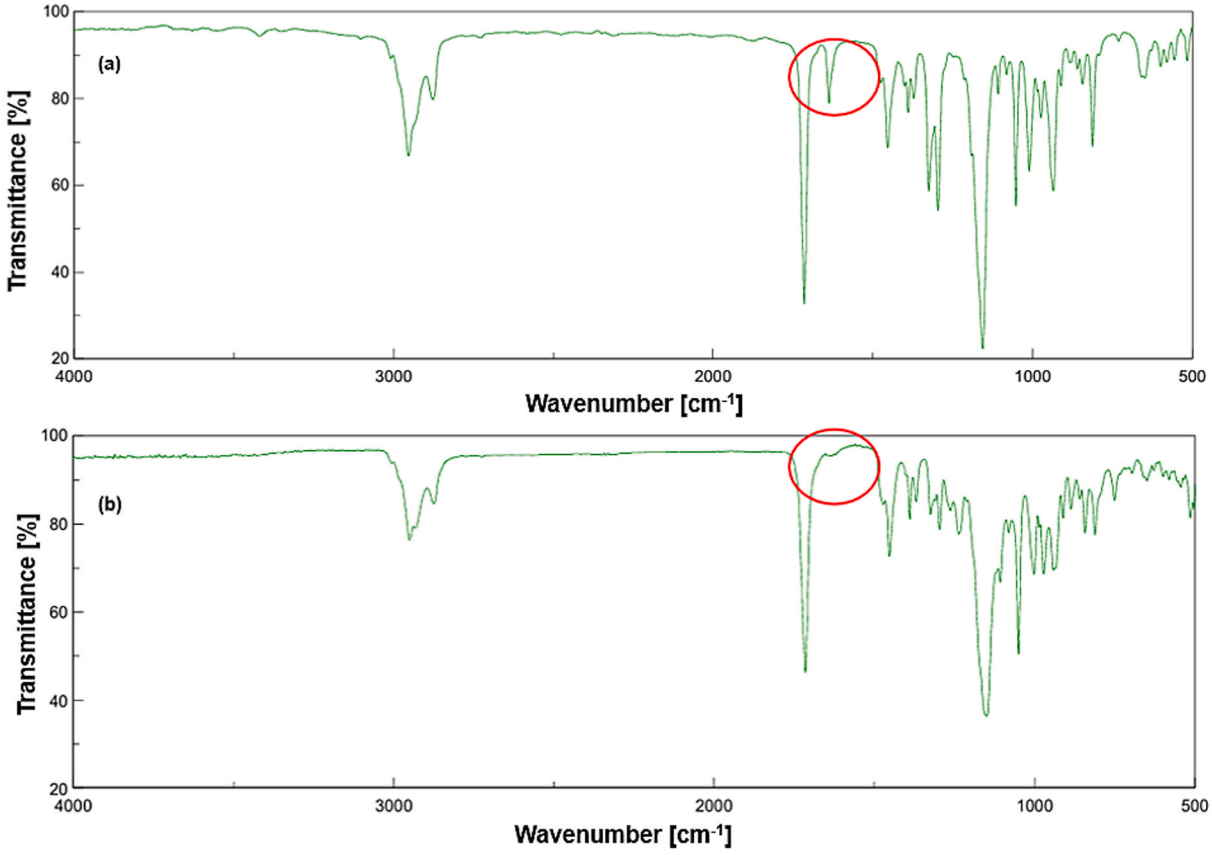


Fig. 3. FTIR spectra of IBOMA (a) and polyIBOMA (b). The graphs highlight the area corresponding to the absorption peak of the C=C bond. In the monomer spectrum the peak is clearly visible, while in the polymer spectrum it disappears.

FTIR spectroscopy

FTIR spectroscopy was conducted on the monomers, polymers, and copolymers to monitor the intensity of the characteristic double-bond peaks of IBOA and IBOMA, thereby evaluating the degree of monomer-to-polymer conversion during UV polymerization step. As an example, Fig. 3a shows the spectrum of the IBOMA monomer: it exhibits a sharp characteristic band at 1637 cm^{-1}, corresponding to the C=C double bond stretching vibration. In contrast, this peak completely disappears in the spectrum of the polymerized sample (Fig. 3b). The disappearance of the vinyl signal provides clear evidence of the successful consumption of the monomeric double bonds, confirming that the UV-curing process reached a high degree of conversion. The same results were obtained for the other (co)polymers used in this work.

Refractive index

A crucial requirement for achieving high optical transparency in wood-based composites is the precise matching of refractive indices between the infiltrating polymer and the delignified wood scaffold. The delignified wood template, primarily composed of cellulose nanofibers, possesses a specific refractive index, and the value reported in the literature (1.53) [5] is approximately the same to that obtained for our delignified samples (1.54). If the refractive index of the chosen polymer differs significantly from that of the cellulose scaffold, light scattering occurs at the interfaces, resulting in an opaque or translucent appearance. Consequently, measuring and selecting a polymer with a refractive index that coincides with the wood matrix is fundamental to ensure maximum light transmittance. The experimental results, summarized in Table 1, confirm that all synthesized samples possess refractive indices closely aligned with the cellulosic scaffold. This optimal index matching indicates that the developed polymeric matrices are highly suitable for the fabrication of TW composites, as confirmed by the appearance of the samples, shown in Fig. 4. In all cases, the underlying pattern remains readily visible through the composite samples.

UV-Vis analysis

To further investigate the optical properties of TW samples, the wavelength-dependent optical transmittance and haze spectra of TW infiltrated with polyIBOA, polyIBOMA, and their copolymer formulations were carried out and reported in Fig. 5. All samples exhibit a sharp increase in transmittance above approximately 350-400 nm, followed by a broad plateau across the visible region (Fig. 5a). This behavior indicates that absorption losses become negligible at longer wavelengths and that light propagation is mainly governed by scattering phenomena within the wood/polymer composite structure.

The hybrid polyIBOA/polyIBOMA formulations display consistently higher transmittance than the corresponding homopolymer systems (Fig. 5a). The three copolymer formulations exhibit comparable transmittance in the visible region, reaching approximately 79–80% at 550 nm, whereas pure polyIBOMA exhibits the lowest value. The higher total transmittance of the copolymer systems may be consistent with differences in infiltration quality and local scattering, although the present data do not establish a unique origin.

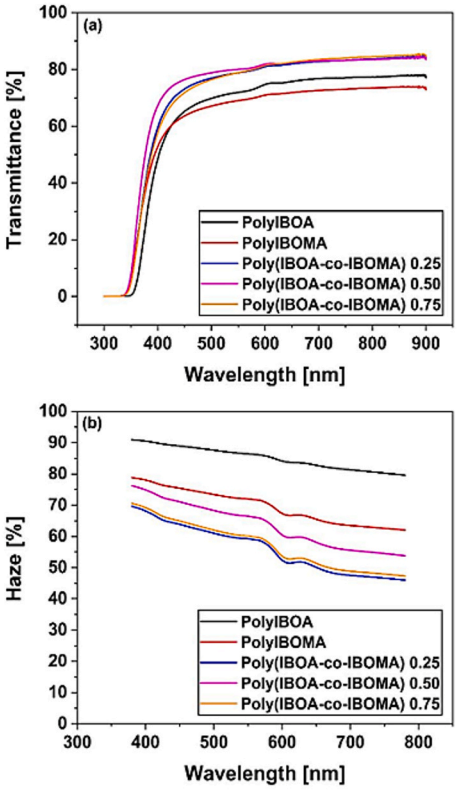


Fig. 5. Spectral optical properties of TW based on polyIBOA, polyIBOMA and their copolymers: (a) optical transmittance and (b) haze as a function of wavelength. For copolymers, the IBOA molar fraction is indicated in the legend.

The haze spectra decrease with increasing wavelength (Fig. 5b), indicating that scattering remains important across the visible region. Compared with the homopolymers, the copolymers generally reduce haze while maintaining high transmittance.

A weak but reproducible spectral inflection is observed around ~600 nm in several samples. Since lignin-related absorption is mainly confined below 450 nm, this feature is unlikely to originate from residual chromophoric species [31]. Instead, it is more plausibly associated with wavelength-dependent scattering effects arising from multiscale structural heterogeneities and slight local refractive index mismatches within the composite architecture [32].

To facilitate comparison among formulations, transmittance and haze values at 550 nm are summarized in Table 2.

Overall, all TW samples exhibit relatively high optical transmittance (approximately 69-80%), confirming an effective suppression of internal attenuation after polymer infiltration. At the same time, haze values remain significant (approximately 59-86%), highlighting the intrinsic scattering nature of the anisotropic wood template.

The three copolymer compositions exhibit comparable transmittance at 550 nm, while the 0.25/0.75 and 0.75/0.25 formulations show lower haze than the 0.50/0.50 composition. Thus, within the investigated compositional range, the main composition-dependent differences are

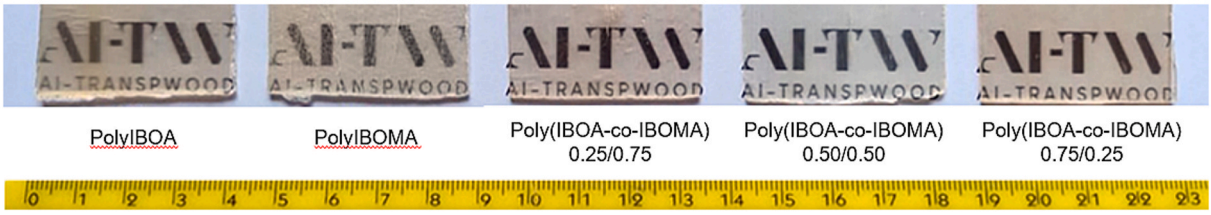


Fig. 4. Typical images of TW samples containing polyIBOA, polyIBOMA and their copolymers.

Table 2
Optical transmittance and haze at 550 nm for TW infiltrated with polyIBOA/polyIBOMA systems measured along the longitudinal direction.

Infiltrating polymer	Average thickness [mm]	Optical transmittance [%]	Haze [%]
PolyIBOA	2.08	71.9	86.44
PolyIBOMA	2.01	69.0	71.99
Poly(IBOA-co-IBOMA) 0.25/0.75	1.96	78.8	59.22
Poly(IBOA-co-IBOMA) 0.50/0.50	1.98	80.0	66.43
Poly(IBOA-co-IBOMA) 0.75/0.25	2.02	78.9	60.13

observed in light diffusion rather than in total optical transmittance.

Scanning electron microscopy

Fig. 6 shows the typical SEM images of the TW cross-sections for polyIBOA, polyIBOMA and the copolymer with molar fraction of polyIBOA equal to 0.50. Their morphology revealed a homogeneous distribution of the polymer matrix within the wood cell walls. These observations indicate extensive polymer distribution within the wood structure while preserving the overall cellular architecture.

Thermal conductivity tests

Table 3 collects the thermal conductivity data for the investigated TW systems. The measured values range from 0.15 to 0.18 $W{\cdot}m^{-1}{\cdot}K^{-1}$, indicating relatively minor variations among the investigated formulations. In addition, the reported values are consistent with the literature for TW derived from balsa, which typically reports k values between 0.20 and 0.30 $W{\cdot}m^{-1}{\cdot}K^{-1}$ [33,34]. The samples infiltrated with the neat IBOA and IBOMA monomers exhibit thermal conductivities of 0.15 ± 0.01 and 0.16 ± 0.01 $W{\cdot}m^{-1}{\cdot}K^{-1}$, respectively. These values are very close, suggesting that the chemical differences between the corresponding polymer matrices only marginally affect the heat transport within the TW structure. Among the copolymer formulations, the TW with poly(IBOA-co-IBOMA) 0.25/0.75 sample shows the highest thermal conductivity (equal to 0.18 ± 0.01 $W{\cdot}m^{-1}{\cdot}K^{-1}$), while the TW with 0.50/0.50 and 0.75/0.25 compositions exhibit values comparable to those of the neat polymer systems (0.15 ± 0.02 $W{\cdot}m^{-1}{\cdot}K^{-1}$ and 0.15 ± 0.01 $W{\cdot}m^{-1}{\cdot}K^{-1}$, respectively). Given the relatively small standard deviations and the narrow conductivity range, these results seem to indicate that the thermal transport properties are mainly governed by the wood/polymer architecture rather than by the specific composition of the polymer phase. More specifically, the overall thermal conductivity is strongly affected by factors like infiltration efficiency, wettability of inner cell walls by the infiltrating monomer, and residual porosity as well. It is possible that minor variations in infiltration quality or local microstructure may be responsible for the observed differences.

Four-point bending tests

Fig. 7 shows the results of the four-point bending tests, in terms of bending stiffness E_b and bending strength σ_b. Given the sandwich-type sample, apparent total stiffness E_{total} and core stiffness E_{core} are discussed, as well as the strength counterpart σ_{total} and σ_{core}. Native balsa exhibited the lowest bending stiffness of approximately 1.5 [35]. All infiltrated samples exhibited a roughly two to three times higher bending stiffness and bending strength, respectively. This behavior agrees with observations reported in previous studies on TW [36]. In these materials, the polymer phase promotes a more efficient transfer of stress between adjacent wood cell walls, resulting in an increased stiffness of the composite structure.

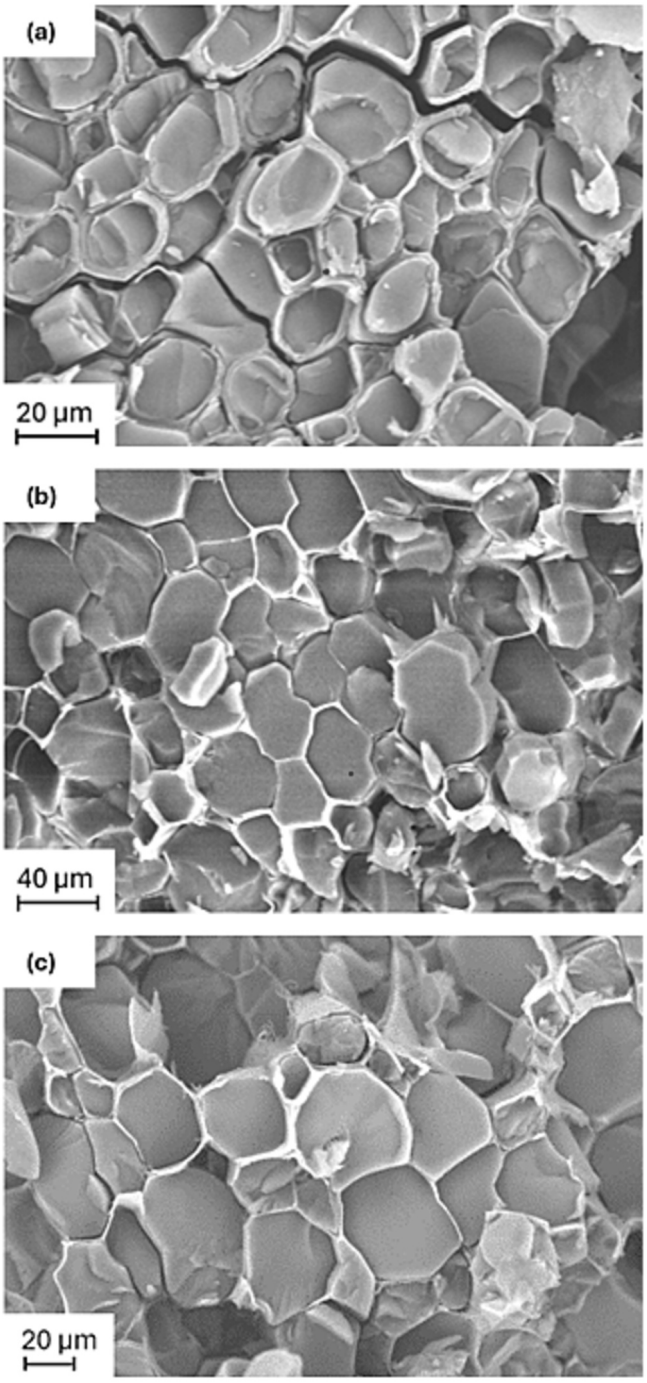


Fig. 6. Cross-sectional SEM image of TW samples embedded with (a) polyIBOA, (b) polyIBOMA, and (c) copolymer containing an IBOA molar fraction of 0.50.

In general, $E_{core} > E_{total}$, showing that the inclusion of the outer polymer layers in the calculation reduces the apparent bending modulus. Only for the 50/50 copolymer, the measured total modulus was below the assumed polymer modulus, leading to a smaller core modulus. The comparison between both evaluation methods indicates that these polymer surface layers indeed need to be accounted for, when aiming at quantifying the TW stiffness.

As expected from the laminate geometry, the absolute E_{core} estimates depended on the assumed modulus of the polymer-rich surface layers. Over $E_{IBOMA}/E_{IBOA} = 0.5$ - 1.0, the estimated E_{core} ranges were 3.78 - 6.29 GPa for polyIBOMA, 6.55 - 6.82 GPa for poly(IBOA-co-IBOMA)0.75,

Table 3
Results of thermal conductivity measurements performed on balsa wood infiltrated with different (co)polymers.

Infiltrating polymer	Thermal conductivity W/(m·K)	Standard deviation
PolyIBOA	0.15	0.01
PolyIBOMA	0.16	0.01
Poly(IBOA-co-IBOMA) 0.25/0.75	0.18	0.01
Poly(IBOA-co-IBOMA) 0.50/0.50	0.15	0.02
Poly(IBOA-co-IBOMA) 0.75/0.25	0.15	0.01

2.42 - 3.62 GPa for poly(IBOA-co-IBOMA)0.5 and 3.75 - 5.57 GPa for poly(IBOA-co-IBOMA)0.25. The variation of the assumed polymer-layer stiffness had no influence on the polyIBOA samples, since E_{IBOA} was obtained from nanoindentation. For samples with increasing polyIBOMA content, the sensitivity increased, as the assumed E_{IBOMA} contributes more to E_{poly}. This is reflected by the ranges obtained from the sensitivity analysis of E_{core}, shown by the grey shaded area, for the polyIBOMA and IBOMA-rich co-polymer samples, whereas the IBOA-rich co-polymer was only weakly affected. Nevertheless, the corrected values showed the same overall trend as the uncorrected bending moduli. Accordingly, E_{total} is used for the quantitative comparison among formulations, whereas E_{core} is reported as a model-dependent range illustrating the influence of the polymer-rich surface layers.

PolyIBOA samples and those containing 0.75 IBOA molar fraction showed the highest total bending stiffnesses among the infiltrated samples. For both evaluation methods, the IBOA-rich samples exhibited higher stiffness values than the samples with a polyIBOMA content equal to or higher than 0.50. The polyIBOA samples showed the highest E_{core}, although the standard deviation was also the largest for this series. The 0.50/0.50 polymer combination resulted in the lowest bending modulus among the infiltrated samples for both evaluation methods. In addition, these samples already exhibited cracks before testing, indicating that this polymer ratio is not suitable for mechanical applications. The cracks may reasonably arise from curing-induced residual stresses, potentially associated with polymerization shrinkage and/or differences in curing kinetics. As the polyIBOMA content increased beyond 0.50, the stiffness increased again, and the polyIBOMA samples also showed slightly higher stiffness. However, their bending moduli remained below those of the samples with higher polyIBOA molar fractions.

As previously observed for the modulus, accounting for the outer polymer layer leads to a reduction in the calculated bending strength values. The core bending strength results show a more distinct trend among the different polymer combinations with respect to the bending

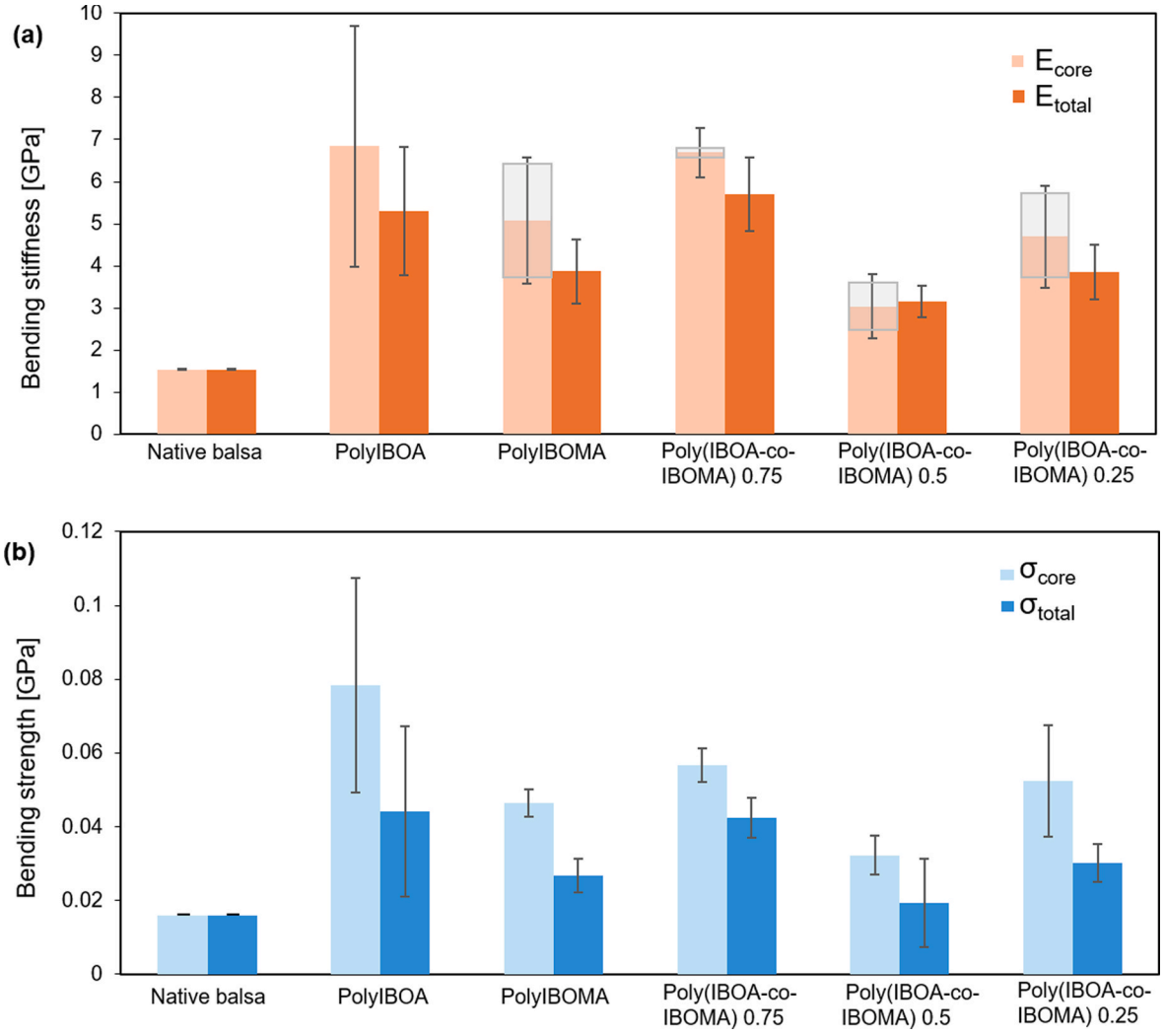


Fig. 7. (a) Bending stiffness and (b) bending strength of the total sample and the TW core, respectively, for native balsa and TW samples containing polyIBOA and/or polyIBOMA. The grey shaded area indicates the variation in the calculated E_{core} caused by varying the assumed polymer-layer stiffness. For copolymers, the IBOA molar fraction is indicated in the x-axis.

stiffness results. The TW samples infiltrated with polyIBOA exhibited the highest bending strength of approximately 0.078 GPa. With increasing polyIBOMA volume fraction, the bending strength gradually decreased to approximately 0.046 GPa for polyIBOMA samples. Only the samples with the 0.50/0.50 molar fraction exhibited an even lower bending strength of approximately 0.032 GPa.

The relatively large error bars may be attributed to variations in the degree and homogeneity of polymer infiltration, the presence of trapped air or residual voids, local differences in polymerization and curing, variations in wood-polymer interfacial adhesion, and the inherent structural heterogeneity of wood-based specimens [2,36]. To further optimize this aspect, dedicated studies will be required to systematically investigate the specific contribution of these parameters and identify the conditions that ensure more reproducible and homogeneous composite microstructures. Consequently, the bending results should primarily be interpreted in terms of the overall trends among the investigated formulations, rather than as evidence for statistically significant differences between formulations whose error bars overlap.

Comparable increases in modulus and strength have been observed in PMMA and epoxy resin-based TW composites, where polymer infiltration improves the load-bearing capability of the resulting composite [5,37,38]. These data confirm that the mechanical response of TW arises from the combined roles of its constituents: the cellulose scaffold retains its reinforcing function, while the polymer fills the porosity and thus facilitates load transfer between the wood cell walls. As a result, the composite exhibits high stiffness without the brittle behavior typically associated with rigid materials [1].

Ultrasound tests

Fig. 8 shows the results of ultrasound tests, with the values of C_{rrrr}, C_{rlrl}, and C_{rtrt} components. The ultrasonic measurements indicate that the choice of polymer has only a negligible influence on the stiffness components associated with wave propagation in the radial direction. The radial normal stiffness C_{rrrr} remained approximately constant at 6 GPa, and only minor differences were observed in the shear stiffness components C_{rlrl} and C_{rtrt}. Irrespective of the polymer system, the shear stiffness components were substantially lower than the radial normal stiffness. The resulting hierarchy, $C_{rrrr} > C_{rlrl} \approx C_{rtrt}$, is consistent with the orthotropic elastic behavior of wood reported in previous ultrasonic studies [29,39,40].

Comparison with literature-reported transparent wood systems

To place the performance of the present isobornyl-based matrices in a broader context, Table 4 compares representative transparent wood systems based on PMMA, PVA/PVOH, and PVP. The literature data should be regarded as benchmarks rather than as a direct quantitative ranking, because wood species, specimen thickness, processing route, measurement wavelength, and mechanical test mode differ among studies. Nevertheless, the comparison highlights a favorable overall balance for the present systems. Despite their larger final thickness (approximately 2.0 mm, compared with about 0.7–1.2 mm for the selected literature examples), the isobornyl-based TW samples retain visible transmittance values of 69–80%, while the 0.25/0.75 and 0.75/0.25 copolymers show haze values close to 60%. For comparison, the classical PMMA/balsa system reported 85% transmittance and 71% haze at 1.2 mm [5], whereas PVP-, PVOH-, and PMMA-infiltrated rubber wood showed transmittance values of 73.4%, 76.6%, and 64.6%, respectively, at thicknesses of about 0.7 mm [10]. The PVA/balsa system reported by Mi et al. represents a particularly high-clarity benchmark (approximately 91% transmittance and 15% haze at 0.8 mm), with a radial thermal conductivity of 0.19 $W{\cdot}m^{-1}{\cdot}K^{-1}$ [33]. The thermal conductivity measured here (0.15–0.18 $W{\cdot}m^{-1}{\cdot}K^{-1}$) is therefore fully competitive from an insulation perspective. Mechanical values across studies are not directly comparable because the literature benchmarks are mainly based on tensile testing, whereas the present work uses four-point bending; however, the isobornyl-based composites showed a clear reinforcement relative to native balsa. Overall, the comparison supports the isobornyl family as a competitive bio-based matrix platform when optical, thermal, and mechanical performance are considered together.

Exploratory Pareto-type optical-mechanical analysis

The optical and mechanical results indicate that the preferred formulation depends on the selected performance criterion. For this reason, the data were examined through an exploratory optical-mechanical desirability comparison (Table 5). Regarding mechanical properties, the values of E_{total} and σ_{total} were considered, as they are representative of the material actually obtained. The analysis was not intended as a statistically validated optimization, because only five formulations were available and optical transmittance and haze were reported as formulation mean values. It was used instead to make the trade-offs explicit. The objectives were to maximize transmittance at 550 nm, minimize haze at 550 nm, and maximize bending stiffness and

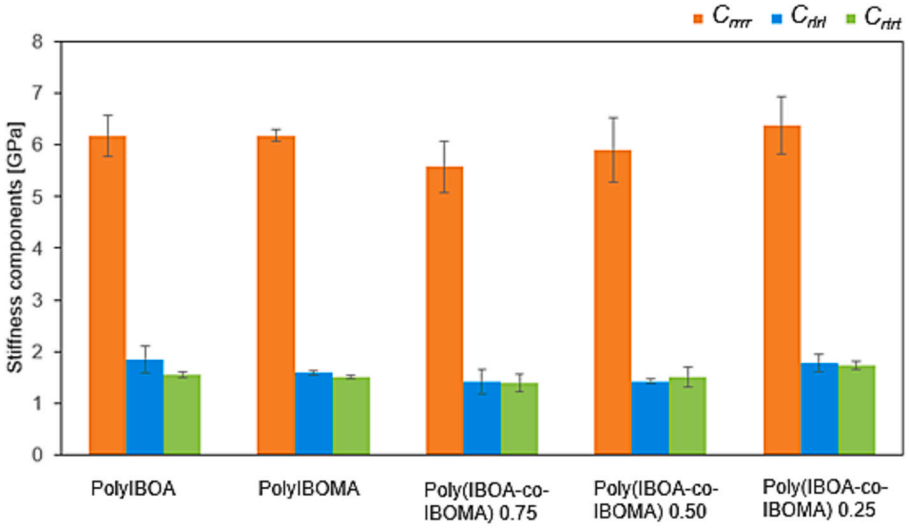


Fig. 8. Shear stiffness components C_{rrrr}, C_{rlrl}, and C_{rtrt} for TW samples containing polyIBOA and/or polyIBOMA. For copolymers, the IBOA molar fraction is indicated in the x axis.

Table 4
Representative comparison of optical, thermal, and mechanical properties of transparent wood based on conventional polymer matrices and the isobornyl-based systems investigated in this work.

Matrix	Wood (thickness)	Transmittance (%)	Haze (%)	k ($W \cdot m^{-1} \cdot K^{-1}$)	Mechanical property	Ref.
polyIBOA/polyIBOMA family	Balsa (1.96–2.08 mm)	69–80 (550 nm)	59–86	0.15–0.18	Bending strength 32–78 Mpa; modulus 3.0 – 6.8 GPa	This work
PMMA	Balsa (1.2 mm)	85 (550 nm)	71	NR[a]	Tensile strength 90 MPa; modulus 3.6 GPa	[5]
PVA	Balsa (0.8 mm)	91 (532 nm)	15	0.19	Tensile strength 143 MPa	[32]
PVP	Rubber wood (0.74 mm)	73.4 (600 nm)	NR[a]	NR[a]	Tensile strength 97 MPa; modulus 7.0 GPa	[10]
PVOH (PVA)	Rubber wood (0.70 mm)	76.6 (600 nm)	NR[a]	NR[a]	Tensile strength 164 MPa; modulus 11.0 GPa	[10]
PMMA	Rubber wood (0.73 mm)	64.6 (600 nm)	NR[a]	NR[a]	Tensile strength 230 MPa; modulus 12.3 GPa	[10]

[a] NR = Not Reported.

Table 5
Exploratory optical-mechanical comparison of the investigated TW formulations. Scores are normalized within this dataset and are intended only as descriptive ranking metrics. The ranking is descriptive and should not be interpreted as evidence of statistically significant differences among formulations.

Formulation	Optical score	Mechanical score	Balanced score	Interpretation
PolyIBOMA	0.27	0.27	0.27	Lowest combined optical-mechanical score
Poly(IBOA-co-IBOMA) 0.25/0.75	0.95	0.63	0.79	Low haze; favorable optical response
Poly(IBOA-co-IBOMA) 0.50/0.50	0.87	0.43	0.65	Comparable transmittance; weaker mechanics
Poly(IBOA-co-IBOMA) 0.75/0.25	0.93	0.95	0.94	Most favorable compromise within the tested series
PolyIBOA	0.13	0.51	0.32	Highest strength; lower stiffness contribution and high haze

bending strength. Thermal conductivity was not included in this comparison because it varied only within a narrow range among the formulations and did not provide sufficient discrimination for the present optical-mechanical ranking. Because the standard deviations of the mechanical results overlap substantially, the resulting mean-value ranking should not be interpreted as evidence of statistically significant differences among formulations.

The formulation mean for each property was normalized between 0 and 1 within the investigated series. For properties to be maximized, the normalized value was calculated as $z = \frac{x - x_{min}}{x_{max} - x_{min}}$; for haze, which was minimized, $z = \frac{x_{max} - x}{x_{max} - x_{min}}$.

Thus, values of 0 and 1 identify only the least and most favorable values observed within this five-formulation dataset and do not represent absolute material limits. The optical score was the arithmetic mean of the normalized transmittance and inverse-haze values, whereas the mechanical score was the arithmetic mean of the normalized bending-stiffness and bending-strength values. The balanced optical-mechanical score was calculated as the equally weighted arithmetic mean of the optical and mechanical scores. Fig. 9 presents this descriptive score for the different polymer formulations.

In this descriptive comparison, polyIBOMA gave the lowest combined optical-mechanical score because its low transmittance was not offset by a superior mechanical response. The 0.50/0.50 copolymer showed transmittance comparable to the other copolymer formulations, but its lower bending stiffness and strength, together with the observed pre-existing cracks, reduced its mechanical score. The 0.25/0.75 and 0.75/0.25 copolymers provided similarly low haze, while the IBOA-rich 0.75/0.25 formulation also showed the highest bending stiffness and a high bending strength. PolyIBOA had the highest bending strength, but this advantage was offset in the equally weighted mechanical score by its lower normalized bending-stiffness contribution. Accordingly, within

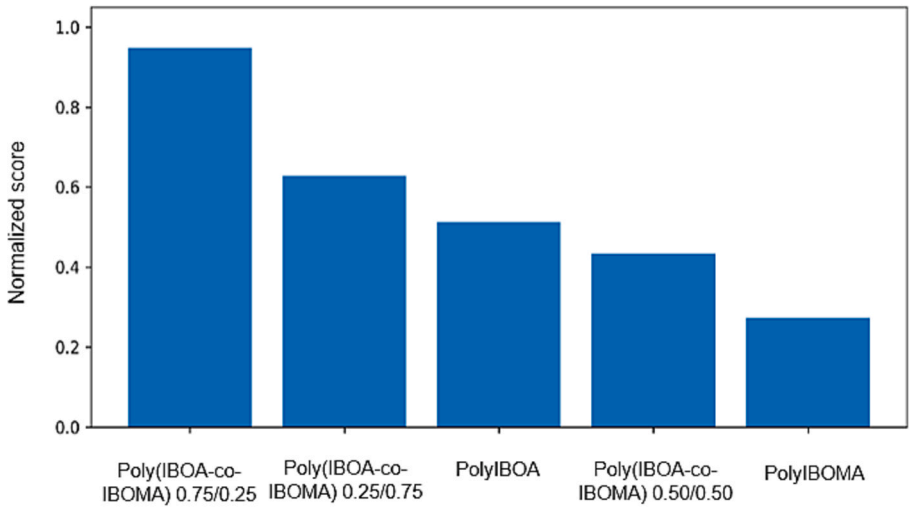


Fig. 9. Exploratory optical-mechanical desirability comparison of the investigated formulations. The balanced score is the equally weighted mean of the normalized optical and mechanical scores and should be interpreted as a descriptive guide to trade-offs, not as a validated optimization metric.

the limits of the present dataset and the stated equal-weighting scheme, the 0.75/0.25 copolymer provided the most favorable overall optical-mechanical compromise rather than a universal optimum for every application.

Conclusions

Transparent wood was prepared using bio-based isobornyl acrylate and isobornyl methacrylate matrices, either as homopolymers or as copolymers.

The measured refractive indices of the polymer films were close to each other and close to the reference value for delignified wood.

The optical response was composition-dependent. At 550 nm, the three copolymer formulations exhibited comparable transmittance, whereas the 0.25/0.75 and 0.75/0.25 copolymers showed lower haze than the 0.50/0.50 composition. These results indicate that variations in the IBOA/IBOMA ratio primarily affect light diffusion rather than total optical transmittance within the investigated copolymer series.

Thermal conductivity remained in a narrow range between 0.15 and 0.18 $W \cdot m^{-1} \cdot K^{-1}$, suggesting that heat transport is governed mainly by the wood-polymer architecture, residual porosity, and infiltration quality rather than by small differences in polymer composition. Mechanical testing showed a stronger dependence on formulation. All infiltrated samples were stiffer than native balsa in longitudinal bending, with the IBOA-rich 0.75/0.25 copolymer and polyIBOA showing the most favorable bending response. The 0.50/0.50 copolymer, despite exhibiting transmittance comparable to the other copolymer formulations, showed the weakest mechanical behavior.

The exploratory optical-mechanical desirability comparison summarizes these trade-offs. PolyIBOMA gave the lowest combined score, while similar transmittance values of the three copolymer formulations indicate that transmittance alone does not provide a meaningful basis for discriminating among them. The 0.25/0.75 copolymer provided the lowest mean haze, but the 0.75/0.25 copolymer gave the most balanced profile when transmittance, haze, bending stiffness, and bending strength were considered with equal optical and mechanical weighting. This comparison is descriptive rather than predictive: the number of compositions is small, and the optical data are reported without uncertainty estimates. The substantial overlap in mechanical-data variability further means that this ranking should not be interpreted as demonstrating statistically significant differences among formulations.

These results support the use of isobornyl-based matrices as bio-based polymer phases for transparent wood, especially when optical and mechanical requirements must be balanced. Within the investigated series, the IBOA-rich 0.75/0.25 copolymer gave the most convincing compromise between optical performance and mechanical integrity.

CRediT authorship contribution statement

Alessia Cabras: Writing – original draft, Visualization, Methodology, Investigation. **Daniele Nuvoli:** Writing – review & editing, Writing – original draft, Visualization, Supervision, Conceptualization. **Giulio Malucelli:** Writing – review & editing, Writing – original draft, Investigation, Conceptualization. **Diego Pugliese:** Writing – review & editing, Writing – original draft, Visualization, Investigation. **Marco Terzi:** Methodology, Investigation. **Markus Königsberger:** Writing – original draft, Methodology. **Johanna Schindler:** Writing – original draft, Visualization, Investigation. **Alberto Mariani:** Writing – review & editing, Writing – original draft, Formal analysis, Conceptualization.

Declaration of competing interest

The authors declare that they have no known competing financial interests or personal relationships that could have appeared to influence the work reported in this paper.

Acknowledgements

The AI-TRANSPWOOD project, HORIZON-CL4-2023-RESILIENCE-01-23 (Grant Agreement 101138191), is gratefully acknowledged. This project is co-founded by the European Union. Views and opinions expressed are however those of the authors only and do not necessarily reflect those of the European Union or HaDEA. Neither the European Union nor the granting authority can be held responsible for them.

Data availability

Data will be made available on request.

References

[1] Jele TB, Andrew J, John M, Sithole B. Engineered transparent wood composites: a review. Cellul 2023;30:5447–71. https://doi.org/10.1007/s10570-023-05239z.
[2] Bradai H, Koubaa A, Zhang J, Demarquette NR. Effect of wood species on lignin-retaining high-transmittance transparent wood biocomposites. Polymers 2024;16:2493. https://doi.org/10.3390/polym16172493.
[3] Xia Q, Chen C, Li T, He S, Gao J, Wang X, et al. Solar-assisted fabrication of large-scale, patternable transparent wood. Sci Adv 2021;7:eabd7342. https://doi.org/10.1126/sciadv.abd7342.
[4] Subba Rao AN, Nagarajappa GB, Nair S, Chathoth AM, Pandey KK. Flexible transparent wood prepared from poplar veneer and polyvinyl alcohol. Compos Sci Technol 2019;182:107719. https://doi.org/10.1016/j.compscitech.2019.107719.
[5] Li Y, Fu Q, Yu S, Yan M, Berglund L. Optically transparent wood from a nanoporous cellulosic template: combining functional and structural performance. Biomacromolecules 2016;17:1358–64. https://doi.org/10.1021/acs.biomac.6b00145.
[6] Zhu M, Song J, Li T, Gong A, Wang Y, Dai J, et al. Highly anisotropic, highly transparent wood composites. Adv Mater 2016;28:5181–7. https://doi.org/10.1002/adma.201600427.
[7] Cai H, Wang Z, Xie D, Zhao P, Sun J, Qin D, et al. Flexible transparent wood enabled by epoxy resin and ethylene glycol diglycidyl ether. J For Res 2021;32:1779–87. https://doi.org/10.1007/s11676-020-01201-.
[8] EFSA J 2015;13:3978–4001. https://doi.org/10.2903/j.efsa.2015.3978.
[9] ECHA (European Chemicals Agency) – Bisphenol A. https://echa.europa.eu/hot-topics/bisphenols. (accessed 10/07/2026).
[10] Yue D, Fu G, Jin Z. Transparent wood prepared by polymer impregnation of rubber wood [*Hevea brasiliensis* Muell. Arg]. BioResources 2021;16:2491–502. https://doi.org/10.15376/biores.16.2.2491-2502.
[11] Haaf F, Sanner A, Straub F. Polymers of N-vinylpyrrolidone: synthesis, characterization and uses. Polym J 1985;17:143–52. https://doi.org/10.1295/polymj.17.143.
[12] Montanari C, Ogawa Y, Olsén P, Berglund LA. High performance, fully bio-based, and optically transparent wood biocomposites. Adv Sci 2021;8:2100559. https://doi.org/10.1002/.202100559.
[13] Purnama P, Samsuri M, Iswaldi I. A review on fully bio-based materials development from polylactide and cellulose nanowhiskers. Polymers 2022;14:4009. https://doi.org/10.3390/polym14194009.
[14] Hai LV, Muthoka RM, Panicker PS, Agumba DO, Pham HD, Kim J. All-biobased transparent-wood: a new approach and its environmental-friendly packaging application. Carbohydr Polym 2021;264:118012. https://doi.org/10.1016/j.carbpol.2021.118012.
[15] Prandato E, Livi S, Melas M, Auclair J, Verney V, Fleury E, et al. Effect of bio-based monomers on the scratch resistance of acrylate photopolymerizable coatings. J Polym Sci Part B 2015;53:379–88. https://doi.org/10.1002/polb.23641.
[16] Badía A, Movellan J, Barandiaran MJ, Leiza JR. High biobased content latexes for development of sustainable pressure sensitive adhesives. Ind Eng Chem Res 2018;57:14509–16. https://doi.org/10.1021/acs.iecr.8b03354.
[17] Chabane N, Dergal F, Pata H, Chikhi I. Synthesis of a bio-based methacrylic polymer using camphor terpene as a renewable resource. Chem Proc 2023;14:89. https://doi.org/10.3390/ecsoc-27-16336.
[18] T. Yuan, Y. Liu, Y. Xiao, X. Li, Z.Y. Yang, Preparation method of isobornyl (meth) acrylate of biological origin, China Patent CN 103304414 A (2020). https://patents.google.com/patent/CN112142593A/en.
[19] Xu XW, Xu XX, Wang SF, Hua Y. Synthesis of isobornyl acrylate in the presence of Amberlyst 15. Chin J Chem Eng 2013;21:282–6. https://doi.org/10.3969/j.issn.0253-2417.2013.03.019.
[20] G. M. Paul, G. Desire, Process for the preparation of isobornyl (meth)acrylate, U.S. Patent US5672733A (1997). https://patents.google.com/patent/US5672733A/en.
[21] López-García MDC, Beebe DJ, Crone WC. Characterization of poly(isobornyl acrylate) as a construction material for microfluidic applications. J Appl Polym Sci 2007;105:1894–902. https://doi.org/10.1002/app.26195.
[22] Yang DS, Cho SH, Yoon SD, Jeong HH, Byun HS. Phase behavior measurement for poly(isobornyl acrylate) + cosolvent systems in supercritical solvents at high pressure. J Supercrit Fluids 2013;79:11–8. https://doi.org/10.1016/j.supflu.2013.01.001.
[23] Gunaydin A, Mugemana C, Grysan P, Federico CE, Dieden R, Schmidt DF, et al. Reinforcement of styrene butadiene rubber employing poly(isobornyl

methacrylate) (PIBOMA) as high Tg thermoplastic polymer. Polymers 2021;13:1626. https://doi.org/10.3390/polym13101626.
[24] Zhang XQ, Wang CH. Solution characterization of poly(isobornyl methacrylate) in tetrahydrofuran. J Polym Sci Part B 1994;32:1951–6. https://doi.org/10.1002/polb.1994.090321112.
[25] ASTM International, Standard Test Method for Haze and Luminous Transmittance of Transparent Plastics (ASTM D1003-21) (2021). https://store.astm.org/d1003-21.html, 2021 (accessed 25 May 2026).
[26] International Organization for Standardization, Plastics — Determination of thermal conductivity and thermal diffusivity — Part 2: Transient plane heat source (hot disk) method (ISO Standard No. 22007-2:2022). https://www.iso.org/standard/81836.html, 2022 (accessed 10 July 2026).
[27] C. Mittelstedt, Laminat- und Sandwichträger, in: C. Mittelstedt (Ed.), Rechenmethoden des Leichtbaus: Grundlagen, Stäbe und Balken, Energiemethoden, Springer, Berlin, Heidelberg, 2021, pp. 645–670. https://doi.org/10.1007/978-3-662-62720-4_18.
[28] Patel MP, Braden M. Heterocyclic methacrylates for clinical applications: I. Mechanical properties, Biomaterials 1991;12:645–8. https://doi.org/10.1016/0142-9612(91)90110-v.
[29] Kohlhauser C, Hellmich C, Vitale-Brovarone C, Boccaccini AR, Rota A, Eberhardsteiner J. Ultrasonic characterisation of porous biomaterials across different frequencies. Strain 2009;45:34–44. https://doi.org/10.1111/j.1475-1305.2008.00417.x.
[30] Schneider HA, Rieger J, Penzel E. The glass transition temperature of random copolymers: 2. Extension of the Gordon-Taylor equation for asymmetric Tg vs composition curves, Polymer 1997;38:1323–37. https://doi.org/10.1016/S0032-3861(96)00652-0.
[31] Li Y, Fu Q, Yang X, Berglund L. Transparent wood for functional and structural applications. Philos Trans A Math Phys Eng Sci 2018;376:20170182. https://doi.org/10.1098/rsta.2017.0182.
[32] Vasileva E, Chen H, Li Y, Sychugov I, Yan M, Berglund L, et al. Light scattering by structurally anisotropic media: a benchmark with transparent wood. Adv Opt Mater 2018;6:1800999. https://doi.org/10.1002/adom.201800999.
[33] Mi R, Li T, Dalgo D, Chen C, Kuang Y, He S, et al. A clear, strong, and thermally insulated transparent wood for energy efficient windows. Adv Funct Mater 2020;30:1907511. https://doi.org/10.1002/adfm.201907511.
[34] Liu S, Tso CY, Lee HH, Du YW, Yu KM, Feng SP, et al. Self-densified optically transparent VO_2 thermochromic wood film for smart windows. ACS Appl Mater Interfaces 2021;13:22495–504. https://doi.org/10.1021/acsami.1c03803.
[35] Easterling KE, Harrysson R, Gibson LJ, Ashby MF. On the mechanics of balsa and other woods. Proc A 1982;383:31–41. https://doi.org/10.1098/rspa.1982.0118.
[36] Farajzadeh Moshtaghin A, Franke S, Keller T, Vassilopoulos AP. Experimental characterization of longitudinal mechanical properties of clear timber: Random spatial variability and size effects. Constr Build Mater 2016;120:432–41. https://doi.org/10.1016/j.conbuildmat.2016.05.109.
[37] Jungstedt E, Montanari C, Östlund S, Berglund L. Mechanical properties of transparent high strength biocomposites from delignified wood veneer. Compos - A: Appl Sci Manuf 2020;133:105853. https://doi.org/10.1016/j.compositesa.2020.105853.
[38] Le Duc T, Thanh-Long N, Huong NTM, Hai NT, Thang CN, Huong TTT. Fabrication of transparent wood by impregnation of epoxy resin into modified balsa wood for application in energy saving materials. Vietnam J Catal Ads 2025;14:45–50. https://doi.org/10.62239/jca.2025.009.
[39] V. Bucur, The Acoustics of Wood, third ed., CRC Press, Boca Raton, 2025. https://doi.org/10.1007/947-3-662-03124-7.
[40] R.J. Ross, Nondestructive Evaluation of Wood, second ed., USDA Forest Service, Forest Products Laboratory, General Technical Report FPL-GTR-238, Madison, WI, 2015, 176 pp. https://doi.org/10.2737/FPL-GTR-238.